Journal of Solid State Chemistry **162,** 220–224 (2001)
doi:10.1006/jssc.2001.9255, available online at http://www.idealibrary.com on IDEAL®

$AgCuO_2$—Synthesis, Crystal Structure, and Structural Relationships with CuO and $Ag^{I}Ag^{III}O_2$

J. Curda, W. Klein, and M. Jansen[1]

Max-Planck-Institut für Festkörperforschung, Heisenbergstr. 1, D-70569 Stuttgart, Germany

Received February 15, 2001; in revised form May 16, 2001; accepted May 25, 2001; published online July 26, 2001

IN HONOR OF PROFESSOR PAUL HAGENMULLER ON THE OCCASION OF HIS 80TH BIRTHDAY

The new silver cuprate $AgCuO_2$ was synthesized by applying a low-temperature route. $AgCuO_2$ precipitates as a microcrystalline black and thermally labile powder from concentrated aqueous solutions of copper and silver nitrate under alkaline and oxidizing conditions. Using the positional parameters of $AgAgO_2$ as a starting set, Rietveld refinements have been performed using X-ray and neutron powder data ($P2_1/c$, $a = 5.8657(3)$, $b = 2.8062(2)$, and $c = 6.0770(3)$ Å, $\beta = 108.106(4)^\circ$, $Z = 2$, $R_p = 6.61\%$, $R_{wp} = 5.00\%$ for joint refinement). The crystal structure consists of chains of ladder-like CuO_4 rectangles running along [010], interconnected by AgO_2 dumbbells. For physical and crystal chemical reasons the oxidation states + I for silver and + III for copper, respectively, have been assigned. Similar to $AgAgO_2$ and CuO the metal cations form a fcc structure with oxygen at positions slightly displaced from the centers of the octahedral vacancies. The small differences from the $AgAgO_2$ structure can be traced back to a different off-center position in the octahedral void.

Key Words: **silver cuprate(III); silver oxide; copper oxide; Rietveld refinement.**

INTRODUCTION

Within group 11 of the periodic table, the principle of homology is violated in several respects. For instance, one can take the monoxides, of which the copper representative is rather stable (1), while AgO is thermally labile (2), and no gold monoxide exists at all. Most striking are the fundamentally distinct valence states of copper and silver in these oxides. Divalent, thus paramagnetic, copper is localized on one independent crystallographic site and is coordinated by 4 + 2 oxygen atoms forming a heavily elongated octahedron, in accordance with the Jahn–Teller theorem (3). Quite differently, $Ag^{I}Ag^{III}O_2$ shows charge disproportionation and has to be regarded as a pseudo-ternary oxide (4). The oxidation states can be unambiguously assigned to the different sites by the characteristic shapes of the respective first coordination spheres, linear for silver(I) and square planar for silver(III). This assignment is in agreement with $Ag^{I}Ag^{III}O_2$ being diamagnetic. The marked discontinuity in the group systematics, as revealed by comparing CuO and "AgO", can be traced back to the second ionization potential, which among the coinage metals is highest for silver. Because of the relevance of these features to the understanding of superconductivity in copper oxides we have undertaken investigations aiming at partial substitution of silver for copper in CuO, and of copper for silver in AgO, respectively. If in the desired ternary silver copper oxides disordered 2 + /3 + mixed valencies were achieved, one could expect, as another attractive perspective, such phases to show a transition to a superconducting state. However, Ag_3O_4, which thus far is the only silver oxide known to contain divalent and tervalent silver at the same time, remains paramagnetic and does not show a transition into a superconducting state down to 3.8 K (5, 6).

Since the desired oxides will be thermally labile, it is advisable to employ soft synthetic approaches ("chimie douce").

EXPERIMENTAL

Synthesis. Microcrystalline samples of $AgCuO_2$ precipitate from combined saturated aqueous solutions of 1.205 g (5 mmol) of $AgNO_3$ (Merck, 99%) and 0.85 g (5 mmol) of $Cu(NO_3)_2 \cdot 3H_2O$ (Merck, 99%) by adding a solution of 3.0 g of KOH and 1.5 g of $K_2S_2O_8$ in 150 ml of water at 90°C. The precipitate was filtered off, washed with deionized water, and dried in air at 70°C. Another means of access to $AgCuO_2$ is oxidation of an aqueous suspension of $Ag_2Cu_2O_3$ (7) under the same conditions.

Structure determination. X-ray powder diffraction data were recorded using a STOE-Stadi P diffractometer

[1] To whom correspondence should be addressed. Fax: + 49-711-6891502. E-mail: martin@jansen.mpi-stuttgart.mpg.de.

0022-4596/01 $35.00

TABLE 1
Crystal Data and Structure Determination of $AgCuO_2$

Formula weight	203.413 g/mol			
Space group	$P2_1/c$ (No. 14)			
Unit cell dimensions	$a = 5.8657(3)$ Å			
	$b = 2.8062(2)$ Å			
	$c = 6.0770(3)$ Å			
	$\beta = 108.106(4)^\circ$			
Cell volume	95.075(9) Å^3			
Z	2			
Calculated density	7.105 g/cm^3			
Wave length (X-ray) (Å)	1.540598 (Ge monochromator)			
Data points (X-ray)	8521			
Data points (neutrons)	1151 (bank 1), 2079 (bank 2), 1909 (bank 3)			
Effective 2θ range (X-ray) (°)	10.00–95.00			
Effective d range (neutr.) (Å)	1.0–10.0 (bank 1), 0.5–4.0 (bank 2), 0.4–2.7 (bank 3)			
Refined parameters	24			
R-values	Neutrons Bank 1	Neutrons Bank 2	Neutrons Bank 3	X-ray
R_F^2	5.47%	9.13%	10.37%	5.51%
R_p (20)	2.75%	3.44%	2.81%	6.64%
R_{wp} (20)	3.10%	3.88%	2.86%	9.00%
R_p; R_{wp} (simultaneous refinement)	6.62%; 5.00%			
χ^2 (20)	3.087			

(germanium monochromator, Cu$K\alpha_1$ radiation, $\lambda =$ 154.0598 pm, linear position-sensitive detector, Si as an external standard).

Neutron powder diffraction data were collected by the time-of-flight technique at the ISIS spallation source with the ROTAX diffractometer. A vanadium crucible (diameter = 4 mm) was used as the sample container. The detection was performed by using three He detector banks, which were positioned at $2\theta = 28.75^\circ$ (bank 1), 72.85° (bank 2), and 122.30° (bank 3).

Starting from the structural model of $Ag^{I}Ag^{III}O_2$ the structure has been refined by profile analysis using the Rietveld method [program GSAS (8)]. Essential data of the structure refinements are listed in Table 1. Measured and calculated powder diffraction patterns and the respective difference plots are shown in Figs. 1–4.

Chemical analysis. The cation ratio of $AgCuO_2$ was determined by energy-dispersive X-ray analysis on several samples (Philips ESEM XL30 equiped with a W cathode and an S-UTW-Si(Li) detector, EDAX PV9760/68). The EDX spectra were recorded at an acceleration energy of 25 keV, and the Ag and Cu L-lines were used to calculate the cation concentrations.

Thermal analysis. The thermal behavior was investigated by DTA and TGA (Fig. 5) (STA 429, Netzsch, Selb, Germany); the decomposition products were characterized by X-ray powder diffraction.

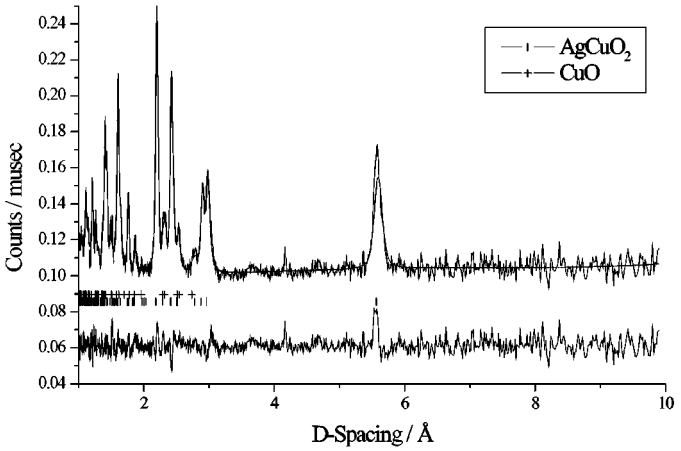

FIG. 1. Neutron diffraction profile fit for $AgCuO_2$ with 5% CuO (bank 1, 28.75°).

Physical properties. The magnetization was recorded using a Squid magnetometer (Quantum Design MPMS; 5–330 K). Measurements of the electrical conductivity of $AgCuO_2$ were performed by the four-point probe method (Van-der-Pauw) on pressed pellets (diameter, 6 mm; thickness, 1 mm),

RESULTS AND DISCUSSION

Applying a low-temperature route, a new ternary silver cuprate, $AgCuO_2$, has been synthesized as a microcrystalline, black powder (Fig. 6). According to EDX microprobe analyses the Ag/Cu ratio amounts to 1:0.99 (average over about five spots per sample, several samples checked). $AgCuO_2$ is insensitive to moisture and can be

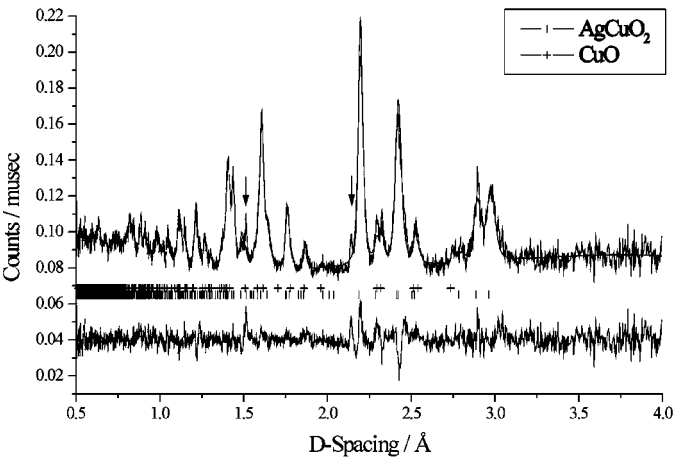

FIG. 2. Neutron diffraction profile fit for $AgCuO_2$ with 5% CuO (bank 2, 72.85°). Reflections caused by vanadium container are marked by arrows.

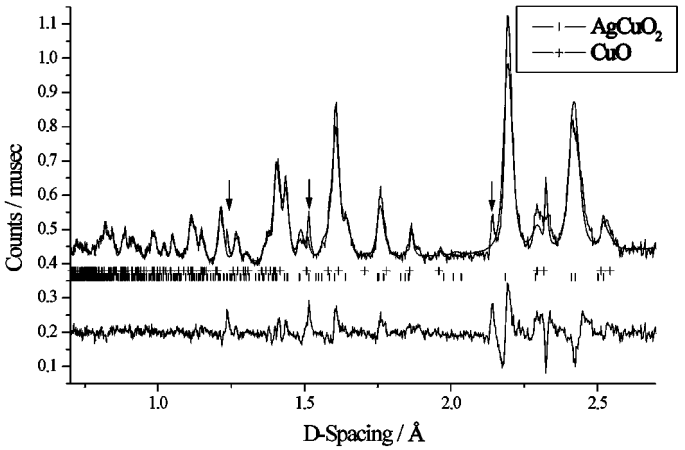

FIG. 3. Neutron diffraction profile fit for $AgCuO_2$ with 5% CuO (bank 3, 122.3°). Reflections caused by vanadium container are marked by arrows.

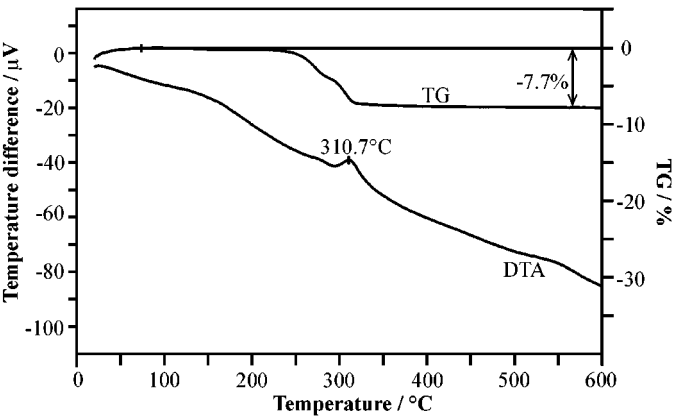

FIG. 5. Combined DTA and TG curves of $AgCuO_2$.

stored undecomposed in air for months. However, it decomposes in an argon atmosphere to a mixture of Ag_2O and CuO within a few days. The thermal degradation, as recorded by thermal analysis, proceeds in two steps at 280°C and 310°C, each accompanied by a loss of oxygen (Fig. 5). The intermediate forming at 280°C has been identified as $Ag_2Cu_2O_3$ (9) by X-ray powder diffraction. The final residue consists of Ag and CuO.

The product phase as obtained via precipitation from an aqueous solution is of mediocre crystallinity, which is reflected by the widths of the powder reflections. Furthermore, among others the sample prepared for the neutron data collection contained small amounts of CuO (cf. Figs. 1–3). Other samples were virtually free of alien phases. Nevertheless, the structural features could be determined unambiguously by fitting X-ray and neutron powder profiles.

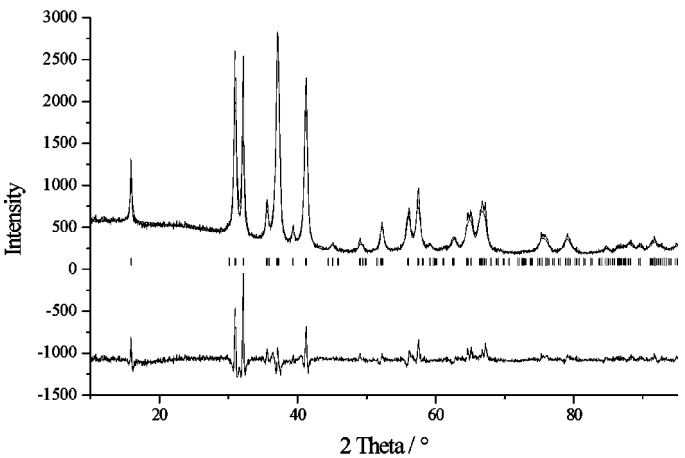

FIG. 4. Rietveld refinement patterns of $AgCuO_2$ (X-ray).

$AgCuO_2$ (Tables 2 and 3; Fig 6) contains silver in a linear coordination by oxygen. The Ag–O bond length 2.178 Å and the O–Ag–O angle 180° are as expected for monovalent silver. Copper is surrounded by four oxygens in a rectangle planar fashion. As the bond lengths (1.871/1.873 Å) are comparable to those found in $NaCuO_2$ (1.839 Å) (10), the oxidation state of 3 + can be assigned to copper. The CuO_4 units are linked via common edges in trans positions, thus forming ladder-like linear chains. As a consequence of this type

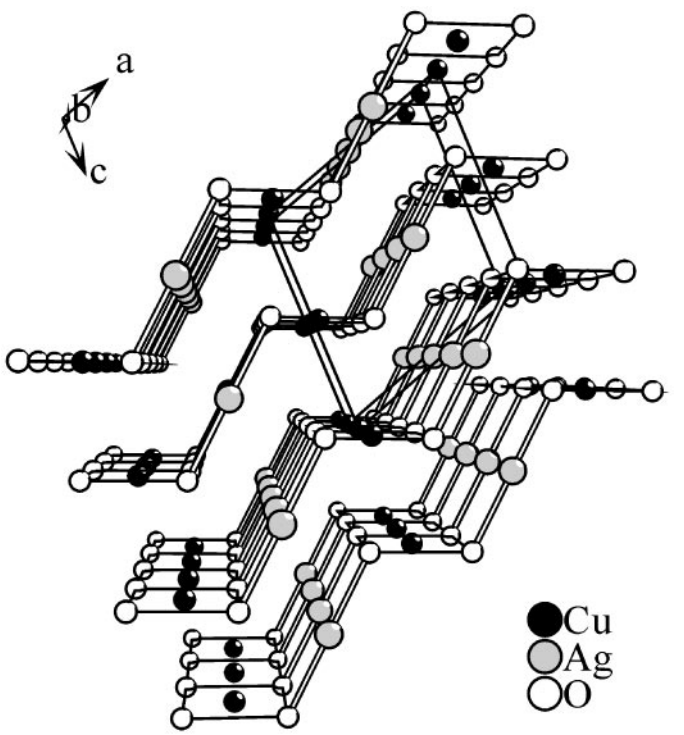

FIG. 6. Crystal structure of $AgCuO_2$.

of connectivity, the O–O spacings at the connecting edges are contracted to 2.461 Å and the corresponding O–Cu–O angles are reduced to 82.93°, as compared to 2.806 Å and 97.07° for the nonconnecting case. All $^2_\infty CuO_2$ chains are running along [010] and are interconnected by AgO_2 dumbbells.

Although the structural features of $AgCuO_2$ and those reported for $Ag^{I}Ag^{III}O_2$ are closely related to each other, the two oxides are not isostructural. Strong similarities in the lattice constants and the positional parameters of the metal atoms in both oxides are obvious; however, under closer inspection, significant differences in the coordinates of oxygen are revealed. These facts can be rationalized when basing the interpretation and comparison of the respective crystal structures on the partial structures of the metal atoms (11–13). These are equal and correspond to an ordered variant of the fcc structure as is similarly realized in the alloy AuCu (14). In either case oxygen occupies the slightly distorted octahedral sites. In $AgCuO_2$, the oxygen atoms are shifted from the center of the octahedral Ag_3Cu_3 voids toward one face, such that the oxygen atoms are receiving two short bonds from copper and one from silver. A shift by a similar amount from the center of the octahedral voids but in another direction results in cardinally different orientations of the AgO_4 squares and AgO_2 dumbbells in $Ag^{I}Ag^{III}O_2$.

At this point, one is becoming aware of a surprisingly general building principle, apparently common to all noble metal oxides containing the metal atoms in linear and/or square planar coordinations. The metal atoms in Cu_2O (15), Ag_2O (16), Cu_4O_3 (17), $Ag_2Cu_2O_3$ (7), CuO (18), $AgCuO_2$, $Ag^{I}Ag^{III}O_2$ (4), or PdO (19) form variants of the fcc structure, which is found in the respective metals, too. Oxygen partly occupies the voids in a way that linear or square coordinations, as favored by the respective cations, result. While in PdO and the metal-rich compounds M_2O and M_4O_3 oxygen enters the tetrahedral sites, in the cases of the MO/M_2O_2 compositions octahedral voids are occupied, establishing a relationship to the rock salt structure.

In agreement with the valence states attributed in terms of structural arguments, $Ag^{I}Cu^{III}O_2$ is diamagnetic and semiconducting with a band gap energy of about 0.2 eV. As mentioned above, $Ag_2Cu_2O_3$ has a face-centered cation arrangement, too. But for transforming $AgCuO_2$ into $Ag_2Cu_2O_3$, a cation rearrangement is necessary, in addition to the loss of oxygen. This fact might explain the different decomposition products obtained at different temperatures. At room temperature binary oxides result from slow decomposition, while at higher temperatures a rearrangement of the cations becomes possible and, accompanied by loss of 25 wt. % oxygen and reduction of Cu(III) to Cu(II), $Ag_2Cu_2O_3$ forms.

A rough estimate of the plausibility of the charge distributions as thus far found experimentally ($Cu^{II}O$, $Ag^{I}Ag^{III}O_2$, and $Ag^{I}Cu^{III}O_2$) can be obtained by considerations in the sense of the Born–Haber cycle. The input data for the four couples $M^{I}M'^{III}/M^{II}M'^{II}$ (M, M' = Ag, Cu) are identical for all data concerning oxygen, within each couple and also over different combinations, while the atomization energies of the metals involved are only identical within a given couple. When assuming that the lattice energies gained are comparable among all I/III and II/II combinations,

TABLE 2
Positional and Isotropic (U_{eq})[a] Displacement Parameters (10^{-1} pm^2) for $AgCuO_2$

Atom	x	y	z	U_{eq}
Ag	0	0	0	5.7(7)
Cu	$\frac{1}{2}$	0	$\frac{1}{2}$	5.8(5)
O	0.2969(4)	0.5040(3)	0.3561(4)	15.6(6)

[a] $U_{eq} = \frac{1}{3}(U_{11} + U_{22} + U_{33})$.

TABLE 3
Selected Bond Lengths (Å) and Angles (°) for $AgCuO_2$, $Ag^{I}Ag^{III}O$ (4), and CuO (18)

Atoms	$Ag^{I}Cu^{III}O_2$	$Ag^{I}Ag^{III}O_2$	$Cu^{II}O$
Cu–O	1.8714(1) [2×]	—	1.95 [2×]
	1.8733(1) [2×]		1.961 [2×]
	2.7834(4) [2×]		2.781 [2×]
Ag^{I}–O	2.1778(1) [2×]	2.161 [2×]	—
	2.7089(1) [2×]	2.688 [2×]	
	2.7102(5) [2×]	2.903 [2×]	
Ag^{III}–O	—	2.023 [2×]	—
		2.028 [2×]	
		2.806 [2×]	
Ag–Ag	2.8062(2) [2×]	3.255 [4×]	—
	3.344(0) [4×]	3.361 [2×]	
		3.408 [4×]	
		3.484 [2×]	
Ag^{I}—Cu^{III}	3.249(1) [4×]	—	—
	3.504(1) [2×]		
Cu–Cu	2.8062(2) [2×]	—	2.900 [4×]
	3.344(0) [4×]		3.083 [2×]
			3.172 [2×]
			3.421 [2×]
			4.665 [2×]
O–O	2.461(1)	2.829 [2×]	2.625 [2×]
	2.8062(2) [2×]	2.900 [2×]	2.900 [4×]
Atoms	$Ag^{I}Cu^{III}O_2$	$Ag^{I}Ag^{III}O_2$	$Cu^{II}O$
O–Cu–O	82.926(5)°	—	84.32°
	97.074(5)°		95.68°
O–Ag^{I}–O	180°	180°	—
O–Ag^{III}—O	—	88.58°	—
		91.42°	

TABLE 4
Sums of Ionization Potentials for All Possible Charge Distributions in $MM'O_2$ (M, M' = Ag, Cu), and Their Differences (eV)

	$\sum I_p(M^I/M^{III})$	$\sum I_p(M^{II}/M^{II})$	Δ
Cu/Cu	72.58	56.03	16.55
Ag/Cu	72.43	57.08	15.35
Cu/Ag	71.61	57.08	14.53
Ag/Ag	71.47	58.01	13.46

respectively, one can try and correlate the sums of the ionization potentials (see Table 4) with the observations. The difference in the sum of ionization potentials $\sum I_p(Cu^I/Cu^{III}) - \sum I_p(Cu^{II}/Cu^{II})$ is largest while it is the smallest for the combination Ag/Ag, which is in agreement with the fact that copper forms $Cu^{II}O$ and silver disproportionates to $Ag^IAg^{III}O_2$. The mixed pairs are intermediate, as one would expect, and there is no conclusive clue for predicting the most probable charge distribution. Surprisingly, the charge distribution according to $Cu^IAg^{III}O_2$ which is favored when considering the ionization potentials only is not found experimentally. This indicates on one hand that this approach is probably too simple, and on the other that transitions between all three possible charge distributions in $AgCuO_2$ might be induced by applying different pressures and temperatures. Furthermore, varying the Ag:Cu ratio could lead to interesting intermediate charge distributions, e.g., $Ag^ICu^ICu^{III}_2O_4$ or $Ag^ICu^{II}_2Cu^{III}O_4$.

CONCLUSION

Different from CuO, however, similar to "AgO", ternary $Ag_{0.5}Cu_{0.5}O$ exhibits charge ordering and has to be regarded as a silver(I) oxocuprate(III). This assignment of valence states is conclusively supported by characteristic structural features and physical properties. Noticeably, the combination of oxidation states as observed (Ag^+/Cu^{3+}) is related to a higher sum of ionization potentials as compared to the opposite combination Cu^+/Ag^{3+}.

ACKNOWLEDGMENTS

The authors thank E. Bruecher and G. Siegle from MPI Stuttgart for magnetic and conductivity measurements, W. Kockelmann from ISIS for recording neutron time-of-flight spectra and R. Hagenmayer for assistance in fitting of the neutron data.

REFERENCES

1. G. Tunell, E. Posnjak, and C. J. Ksanda, *Z. Kristallogr.* **90,** 120 (1935).
2. J. A. McMillan, *J. Inorg. Nucl. Chem.* **13,** 28 (1960).
3. S. Åsbrink and A. Waśkowska, *J. Phys. Condens. Matter* **3,** 8173 (1991).
4. P. Fischer and M. Jansen, *J. Less-Common Met.* **137,** 123 (1988).
5. B. Standke and M. Jansen, *J. Solid State Chem.* **67,** 278 (1987).
6. B. Standke and M. Jansen, *Angew. Chem.* **98,** 78 (1986); *Angew. Chem., Int. Ed. Engl.* **25,** 77 (1986).
7. K. Adelsberger, J. Curda, S. Vensky, and M. Jansen, *J. Solid State Chem.* **158,** 82 (2001).
8. A. C. Larson and R. B. von Dreele, "GSAS (Generalized Structure Analysis System)." Los Alamos National Laboratory, Los Alamos, NM, 1998.
9. P. Gómez-Romero, E. M. Tejada-Rosales, and M. Rosa Palacín, *Angew. Chem.* **111,** 544 (1999).
10. N. E. Brese, M. O'Keefe, R. B. von Dreele, and V. G. Young, Jr., *J. Solid State Chem.* **83,** 1 (1989).
11. M. Jansen, *Angew. Chem.* **99,** 1136 (1987); *Angew. Chem., Int. Ed. Engl.* **26,** 1098 (1987).
12. A. Vegas, *Crystallogr. Rev.* **7,** 189 (2000).
13. M. O'Keefe and B. G. Hyde, *Struct. Bond.* **61,** 77 (1985).
14. E. Bjerkelund, W. B. Pearson, K. Selte, and A. Kjekshus, *Acta Chem. Scand.* **21,** 2900 (1967).
15. R. Restori and D. Schwarzenbach, *Acta Crystallogr.* **42,** 201 (1986).
16. P. Niggli, *Z. Kristallogr.* **57,** 253 (1922).
17. M. O'Keeffe and J. O. Bovin, *Am. Mineral.* **63,** 180 (1978).
18. N. E. Brese, M. O'Keefe, B. L. Ramakrishna, and R. B. v. Dreele, *J. Solid State. Chem.* **89,** 184 (1990).
19. W. J. Moore and L. Pauling, *J. Am. Chem. Soc.* **63,** 1392 (1941).
20. H. M. Rietveld, *J. Appl. Crystallogr.* **2,** 65 (1969).